Analysis method for detecting topological defect dark matter with a global magnetometer network

Hector Masia-Roig*[a], Joseph A. Smiga†[a], Dmitry Budker[a,b,c], Vincent Dumont[b], Zoran Grujic[d], Dongok Kim[e,f], Derek F. Jackson Kimball[g], Victor Lebedev[d], Szymon Pustelny[h], Theo Scholtes[d,i‡], Yannis K. Semertzidis[e,f], Yun Chang Shin[e], Jason E. Stalnaker[j], Ibrahim Sulai[k], Antoine Weis[d], and Arne Wickenbrock[a]

[a]Helmholtz Institut Mainz, Johannes Gutenberg-Universität, 55099 Mainz, Germany
[b]Department of Physics, University of California, Berkeley, CA 94720-7300, USA
[c]Nuclear Science Division, Lawrence Berkeley National Laboratory, Berkeley, CA 94720, USA
[d]Physics Department, University of Fribourg, Chemin du Musée 3, CH-1700 Fribourg, Switzerland
[e]Center for Axion and Precision Physics Research, IBS, Daejeon 34051, Republic of Korea
[f]Department of Physics, KAIST, Daejeon 34141, Republic of Korea
[g]Department of Physics, California State University — East Bay, Hayward, CA 94542-3084, USA
[h]Institute of Physics, Jagiellonian University, prof. Stanislawa Lojasiewicza 11, 30-348, Kraków, Poland
[i]Leibniz Institute of Photonic Technology, Albert-Einstein-Straße 9, D-07745 Jena, Germany
[j]Department of Physics and Astronomy, Oberlin College, Oberlin, OH 44074, USA
[k]Department of Physics & Astronomy, One Dent Drive, Bucknell University, Lewisburg, Pennsylvania 17837, USA

June 3, 2019

Abstract

The Global Network of Optical Magnetometers for Exotic physics searches (GNOME) is a network of time-synchronized, geographically separated, optically pumped atomic magnetometers that is being used to search for correlated transient signals heralding exotic physics. GNOME is sensitive to exotic spin couplings to, e.g., axionic dark matter. This work presents a data analysis procedure to search for axionic dark matter in the form of topological defects: specifically, walls separating domains of discrete degenerate vacua in the axion field. An axion domain wall crossing the Earth creates a distinctive signal pattern in the network that can be distinguished from random noise. The reliability of the analysis procedure and the sensitivity of the GNOME to domain-wall crossings is studied using simulated data.

1 Introduction

The overwhelming evidence for dark matter [1] has inspired various theories to explain its nature [2, 3]. Many of these theories propose new, undiscovered particles as candidates for dark matter [2, 4], and various

*Corresponding author: hemasiar@uni-mainz.de
†Corresponding author: jsmiga@uni-mainz.de
‡Present address

experiments have been designed to search for these candidates [5–9]. Among the candidates is the QCD axion, a particle that was first introduced as a solution to the strong CP problem [10]. The axion is a promising candidate for dark matter [11] as its existence would not only explain dark matter but could also be connected to multiple other phenomena: such as the aforementioned strong CP problem and the hierarchy problem [8]. In general, dark matter could consist of axion-like particles [12] that are unrelated to the strong CP problem. Hereafter, "axion" will refer to any axion-like particle and not only the QCD axion which possesses a particular constraint on the mass-coupling relationship.

Axions may form topological defects such as domain walls [13,14] or composite objects such as axion stars due to self-interactions [15–18]. In particular, axion domain walls form between spatial domains wherein the axion field is centered around discrete vacua states — so the transition between these vacuum domains must include states that are not locally vacuum states. Axion domain walls are formed during a phase transition as the universe cools through expansion [19]. If the phase transition occurred after inflation, domain walls may continue to exist today; otherwise inflation would have pushed other domains outside of the observable universe. The domain walls may contain a substantial amount of energy, which may explain some component of dark matter [14] and possibly dark energy [20]. These structures are virialized in the galaxy with velocity dispersion of 290 km/s according to the standard halo model (SHM) [21]. In this study, an analysis method is developed to search for axion domain walls using a global network of optical magnetometers.

A coupling of the axion field to ordinary matter may take different forms, as long as such interactions are not forbidden by fundamental laws of physics. For example, fermion spins may couple to the gradient of the axion field [19]. If fermionic matter crosses a region with an axion field gradient, it would experience a transient spin-dependent energy shift. This energy shift would appear as an effective magnetic field in spin-based magnetometers which measure the energy level splitting of different spin states.

To search for such transient spin-dependent effects, optical atomic magnetometers [22] were set up around the Earth to form the Global Network of Optical Magnetometers for Exotic physics searches (GNOME) [23, 24]. At the core of each GNOME magnetometer is a vapor cell containing a gas of spin-polarized atoms. The atomic vapor cells are mounted within multi-layer magnetic shields that isolate them from external magnetic perturbations while retaining sensitivity to exotic fields causing spin-dependent energy shifts [25]. Based on the experimental geometry, each magnetometer is sensitive to fields along a particular spatial axis and relatively insensitive to fields in the plane perpendicular to the sensitive axis. Each magnetometer has a characteristic bandwidth, typically $\sim$ 100 Hz. There are additional sensors (accelerometers, gyroscopes, unshielded magnetometers, laser diagnostics) to monitor data quality. The magnetometers may have down times and data flagged as having poor-quality. For further technical details on the GNOME network characteristics, see Ref. [23].

The analysis presented is designed to be applied on the data from the GNOME network. Therefore, the simulated data generated in this work mimic the characteristics of the GNOME stations. The position, orientation of the sensitive axis, and average noise background of the nine simulated magnetometers are shown in Table 1. The noise background on each magnetometer is estimated by the average standard deviation of 30 min pre-processed data segments from December 2017.

Table 1: Characteristics of the GNOME sensors used for the simulated data. The noise is determined by the average standard deviation of GNOME data from December 2017 after filtering and binning.

Property	Position (Lon, Lat)	Orientation (Az,Alt)	Noise (pT)
Beijing	(116.1867° E, 40.2457° N)	(0°,90°)	10.4
Berkeley	(122.2569° W, 37.8723° N)	(0°,90°)	14.5
Daejeon	(127.3987° E, 36.3908° N)	(0°,90°)	116
Fribourg	(7.1581° E, 46.7929° N)	(-170°,0°)	12.6
Hayward	(122.0539° W, 37.6563° N)	(0°,90°)	14.3
Hefei	(117.2525° E, 31.8428° N)	(90°,0°)	12.0
Krakow	(19.9048° E, 50.0289° N)	(45°,0°)	15.6
Lewisburg	(76.8825° W, 40.9557° N)	(0°,90°)	54.5
Mainz	(8.235° E, 49.9914° N)	(0°,90°)	6.78

If the Earth encounters a domain wall, a distinctive pattern is imprinted in the network. Signals would be found at each station at different times and different amplitudes. Such a pattern is determined by the relative velocity between the Earth and the domain wall and the orientation of the sensors. Phenomenologically, the physical thickness of the domain wall is proportional to the inverse axion mass [19]: the natural length parameter in the problem. These dependencies allow the extraction of the domain-wall event properties; such as velocity, magnitude, and width.

Given data from GNOME, a method is needed to search for signals resulting from the spin coupling to the axion field during a domain-wall crossing. This paper describes a method to find statistically significant signal patterns that are consistent with a wall-crossing event. Additionally, a definition of network sensitivity is established that characterizes the properties of domain-wall signals that are observable by GNOME.

The analysis procedure follows several steps, as described in detail in Sec. 2. The wall velocity determines the timing of the signal at different stations, while the relative orientation between the domain-wall plane and the sensitivity axis of each magnetometer determines the measured amplitude. Potential wall events are found by their amplitude above the noise when considering data from all sensors. Then the signals from each magnetometer are characterized. The timing and amplitude are used to determine statistical consistency with a domain-wall crossing. These methods are tested with simulated data, as described in Sec. 3. These tests inform the choice of appropriate thresholds for finding and verifying a domain-wall event.

2 Analysis procedure

The analysis procedure presented here is designed to search the GNOME data for domain-wall crossing events. These events are modeled as a plane of finite width that travels through the Earth at a particular velocity. For a given plane orientation and speed,[1] the signal pattern in the sensor network can be predicted. Assuming a linear coupling between the axion field gradient and fermionic spins (i.e., of the form $J^\mu \partial_\mu a$ for J^μ related to the fermion spin and a being the axion field [19]), the sensor response will appear as a peak in the time-series data as the domain wall crosses. Although the exact form of the signal is model-dependent, it is assumed to be approximately Lorentzian in this analysis [26]:

$$f(t - t_0) = \frac{\Delta B}{1 + \left(\frac{t - t_0}{\frac{1}{2}\tau}\right)^2} \,. \tag{1}$$

The signal expressed in Eq. (1) is based on the signal observed by the magnetometers at time t_0 where ΔB is the peak amplitude of the effective magnetic field and τ is the full width at half maximum (FWHM) over time; i.e., the signal duration. The peak amplitude observed by an individual sensor is also affected by the specific field coupling to that sensor and signal attenuation due to projecting along the sensitive axis of the sensor. These parameters can be related to, e.g., physical parameter space of axion domain walls.

The analysis procedure is composed of several steps designed to find candidate events and confirm the agreement with a domain-wall crossing. First, the raw data are filtered and binned in order to enhance the signal-to-noise ratio of the expected signal for a certain range of parameters. Second, potential crossing events are identified combining the data from the individual magnetometers into a single time series. Events featuring an amplitude greater than some threshold are flagged. Then, the candidate events are scrutinized for consistency with a planar domain-wall crossing event. Crossing time, duration, and amplitude of the candidate event measured at the different magnetometers are fitted to a model to confirm the detection. This gives rise to a consistency check containing three parameters describing the agreement between the data and the model.

2.1 Data pre-processing

In order to reduce noise for a particular range of signal duration, the data are pre-processed through filtering and binning (see Fig. 1). Filters are used to remove long-term drifts as well as noisy frequency bands, e.g., the power-line frequency [23]. After filtering, the data are averaged into bins of length T to decrease

[1] For an ideal plane, only the velocity perpendicular to the plane is observable. Thus, the velocity is entirely described by the speed and orientation of the wall.

random noise. Binning the data enhances the signal-to-noise ratio for a certain signal duration and avoids complications arising from different magnetometers having different bandwidths. However, filtering and averaging data will also attenuate and modify the shape of Lorentzian signals.

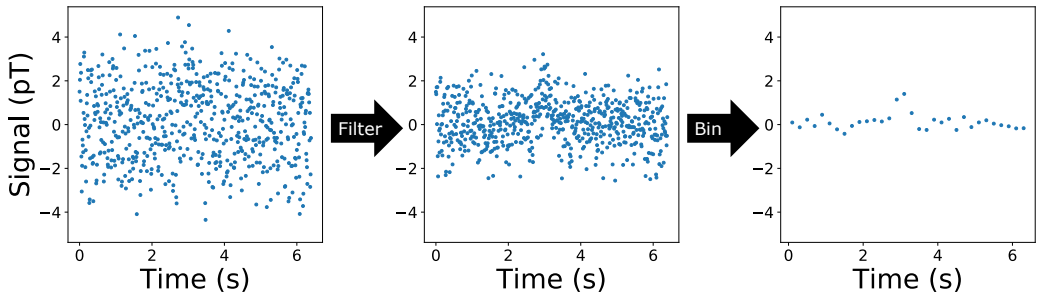

Figure 1: Illustration of data processing on a simulated signal.

First, consider the effects of filtering on the signal. A filter can be represented as a function $\tilde{g}(\nu)$ in frequency space that modifies the frequency-space signal $\tilde{f}(\nu)$ so that the filtered signal in frequency space is $\tilde{f}_{\rm filt}(\nu) = \tilde{g}(\nu)\tilde{f}(\nu)$. As an example, consider a filter $\tilde{g}(\nu)$ defined as $\tilde{g}(\nu) = 0$ for $|\nu| \in \cup_i[\nu_{{\rm L},i}, \nu_{{\rm H},i}]$ and $\tilde{g}(\nu) = 1$, otherwise. In practice, these can include notch filters at 50 Hz and 60 Hz to mitigate the power-line frequencies and a high pass filter to remove drifts. For a Lorentzian signal described in Eq. (1), the amplitude is attenuated by a factor of

$$\epsilon = 1 - \sum_i \left(e^{-\pi\tau\nu_{{\rm L},i}} - e^{-\pi\tau\nu_{{\rm H},i}}\right) \ . \tag{2}$$

The attenuation in Eq. (2) can be derived considering that the Fourier transform of a Lorentzian is of the form $e^{-\pi\tau|\nu|}$.

The data are averaged in bins to increase the sensitivity to peaks, though this improvement is dependent on the bin width. When the binning time T is on the order of the peak duration, the signal-to-noise is maximized. Gaussian distributed random noise is suppressed by averaging the data over a period of time. However, if the binning window is too large, the signal is averaged out. Considering a Lorentz peak contained within a Gaussian distributed noise background, the optimum binning time can be calculated. Binning reduces the noise background $\propto 1/\sqrt{T}$. However, the signal's amplitude is approximately constant for binning windows smaller than the duration of the signal. For binning windows much larger than the duration of the signal, the signal's amplitude is linearly attenuated. In between these two regimes, an optimum can be found. If the signal's peak aligns with the center of a bin, then the maximum signal-to-noise ratio is obtained when $\frac{T}{\tau} \approx 1.4$. Likewise, if the signal falls between two bins, the signal-to-noise is optimized for $\frac{T}{\tau} \approx 0.70$ (exactly half of the previous case). The peak amplitude of the signal S after binning will be in the range

$$\frac{\Delta B\tau}{2T}\tan^{-1}\frac{2T}{\tau} \leq S \leq \Delta B\frac{\tau}{T}\tan^{-1}\frac{T}{\tau} \ . \tag{3}$$

After filtering and binning the data, the Lorentzian shape of the signal is perturbed. However, for typical filters, the filtered signal will be approximately Lorentzian with a slightly different amplitude and width. Thus, Eq. (3) is still approximately true. Moreover, considering binning as a filter, then redundant frequency filters — i.e., those that remove frequency components that are also removed by binning — will not affect Eq. (3).

The filters attenuate frequency bands containing known noise sources, however some non-Gaussian noise from unidentified sources may remain. Therefore, the noise is calculated both before and after the pre-processing steps. The uncertainty at a given time is estimated by the standard deviation of the data around that time. The time interval used to calculate the standard deviation depends on the noise characteristics of the data; e.g., according to the Allan variance.

2.2 Searching for signals

After pre-processing the data, a search algorithm is used to find potential wall-crossing events. The expected signal appears in all magnetometers in a predictable pattern according to the relative velocity and width of the domain-wall crossing. For a given velocity, the data from different sensors can be combined to improve the signal-to-noise ratio. A time shift is applied to compensate for delays between the detection at different locations. Then a weighted mean is calculated based on the directional sensitivity and the noise level of each sensor. The times at which the weighted mean exceeds a chosen signal-to-noise threshold are selected as potential domain-wall crossing times. This way, information from all sensors is used to identify plausible domain-wall events.

The sensors in the network are located at different positions, $\{\boldsymbol{x}_i\}$ on the surface of the Earth. A planar domain wall with speed $\|\boldsymbol{v}\|$ in direction $\hat{\boldsymbol{v}}$ crossing the Earth is observed by different sensors at times $\{t_i\}$. The time difference from when a wall passes two locations can be expressed as

$$\Delta t_i = (\boldsymbol{x}_\mathrm{i} - \boldsymbol{x}_0) \cdot \frac{\boldsymbol{v}}{\|\boldsymbol{v}\|^2} \ , \tag{4}$$

where the sensor at $\boldsymbol{x}_0$ is used as a reference. In addition, each station has a sensitive axis $\hat{\boldsymbol{d}}_i$. This results in an attenuation of the observed wall signal amplitude given by:

$$\kappa_i = \hat{\boldsymbol{d}}_i \cdot \hat{\boldsymbol{v}} \ . \tag{5}$$

The known properties of the dark matter halo are used to model the statistics of domain-wall encounters. The expected domain-wall velocity distribution with respect to the Earth is inferred from the SHM [27]. The SHM assumes that in the galactic rest frame, the velocity distribution of dark-matter objects is isotropic and quasi-Maxwellian, with dispersion ≈290 km/s and maximum speed given by the galactic escape velocity ≈550 km/s [21]. The Earth moves in the dark matter halo at ≈220 km/s with apparent velocity towards the Cygnus constellation. Considering these assumptions 95 % of the walls have speeds between 119 and 599 km/s. Regarding the direction, 95 % of the walls come from a direction contained in a 2π solid angle centered in the forward direction.

Given these dynamics, the delays and attenuation can be calculated. The time of each station's data is shifted to a common location using Eq. (4) so that the time represents when a signal with a particular velocity passes some reference location; in this case the center of the Earth is chosen. This time shift allows individual signals to be combined into a weighted mean in which the signal-to-noise is optimized, $\sum_i w_i s_i$.

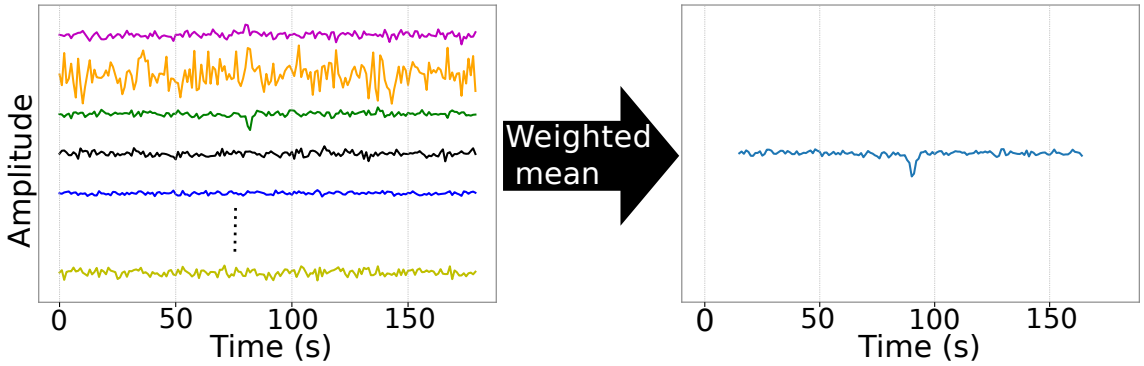

Figure 2: Right: simulated response of nine magnetometers, as characterized in Table 1, to a domain-wall crossing event. Left: the signals measured by different magnetometers. Right: the weighted mean of the shifted signals.

The weighted mean is used to reduce the random noise and to account for the directional sensitivity. The weights are given by

$$w_i = \frac{\kappa_i/\sigma_i^2}{\sum_j \frac{\kappa_j^2}{\sigma_j^2}} \ , \tag{6}$$

where σ_i corresponds to the standard deviation of the noise at the i^{th} station. A signal of strength m is observed by the station as $s_i = \kappa_i m$. The denominator in Eq. (6) normalizes the mean so that $\sum_i w_i s_i = m$. The uncertainty in the weighted mean is then given by

$$\bar{\sigma} = \frac{1}{\sqrt{\sum_i \kappa_i^2/\sigma_i^2}} \ . \tag{7}$$

The weighted mean, after time shifting, is illustrated in Fig. 2.

A weighted sum is performed for a single velocity. Therefore, the possible velocities are scanned to ensure the detection of any domain walls complying with the SHM. The scanning step is estimated considering two antipodal magnetometers. From Eq. (4) the changes in the delay time with respect to variation in the speed can be estimated. However, the delay is also dependent on the direction of the wall. In order to give a upper-bound, the direction giving strongest variation is chosen. In addition, it is imposed that the maximum delay change must be smaller than $\tau/2$, so the signal remains in the same bin. The speed is scanned in steps of

$$\delta v \leq \frac{Tv^2}{4R_\oplus} \ , \tag{8}$$

where $R_\oplus$ is the radius of the Earth. This quantity is used to sample the possible speeds given by the SHM. The same procedure can be followed to establish a scanning steep for the angles. The step is given by

$$\delta\phi \leq \frac{Tv}{4R_\oplus} \ . \tag{9}$$

Note that the scanning step is dependent on the speed. This quantity is used to construct a lattice of points centered away from the direction of Deneb.

When scanning these parameters, a signal is expected in the direction of an incoming domain-wall event, as can be seen in Fig. 3. The left figure shows the signal amplitude found when the same data are analyzed for different directions for a given speed. The polar angle in the figure indicates the angle with respect to the Cygnus constellation. In the right figure, the simulated domain-wall crossing times are randomized for each sensor. A pattern is observed, however it is broader, and the maximum amplitude found has half the strength. Thus, this method enhances signals that reproduce the expected pattern across the network.

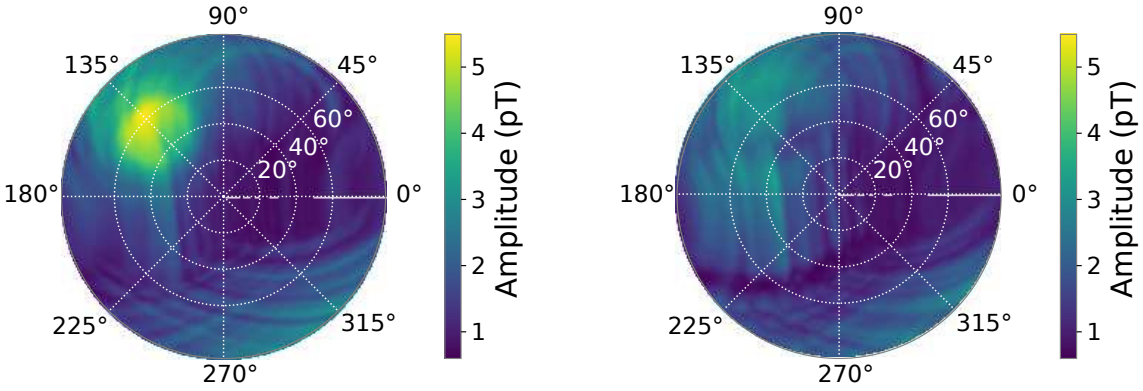

Figure 3: Illustration of the maximum signal amplitude found at different directions, $\hat{v}_{\text{scan}}$, across a single hemisphere. Left: a domain-wall event is inserted in the data with magnitude 5.88 pT and direction at polar angle 60° and azimuthal angle 135°. It correspond to the data shown in Fig. 2. Right: the same domain wall event is insert but the time delays at each magnetometer are randomized. The simulation is performed using the magnetometers' characteristics from Table 1.

A single time series is obtained from the weighted mean for each direction and speed. The values measured are normalized with the standard deviation calculated for the corresponding time series. Data points that differ from the noise background less than a chosen threshold are rejected. Within the remaining data, the direction and speed that yield the greatest deviation from the background is selected. The threshold is determined by a study of the false positive and false negative detection rate as discussed in Sec. 3. The events found are scrutinized for consistency with a domain-wall crossing event.

2.3 Consistency with a domain-wall crossing

After finding a potential events, the data are scrutinized for consistency with the expected signals resulting from a domain-wall crossing event. Using the candidate events from the search algorithm, the signal amplitude, time, and duration are independently extracted from each magnetometer. These parameters are fitted to a domain-wall crossing model to determine the magnitude, speed, and direction of the candidate domain wall. The agreement of the data with the model provides a consistency check as well as two different estimations for the direction of the wall. Agreement between these directions provides another consistency check. Finally, demanding that the signal duration measured at each magnetometer should be in agreement provides an additional consistency check.

These three consistency checks quantify the agreement of the measured signal with a domain-wall crossing event. The agreement is expressed according to the corresponding three p-values; where the p-value is a statistical measure of agreement. Small p-values indicate inconsistency with the model. The specific thresholds placed on these parameters are discussed and determined in Sec. 3 using simulated data.

2.3.1 Characterizing individual signals

The search algorithm, presented in Sec. 2.2, provides information on the velocity and magnitude of the signal. However, it is not sensitive to the specific properties of the signal observed at each magnetometer, such as line-shape, time ordering, and relative amplitude of the signal. In order to extract this information, the data from the individual sensors are independently fitted to Lorentzian peaks.

The initial guess for the time is provided by the search algorithm. However, the domain-wall magnitude found by the search algorithm is not used so that the measurements are less biased to agree with the domain-wall model. The magnitude is estimated by the measurement at the expected signal time in the binned data. The width is determined by the times at which the value drops to half of the value given by the amplitude.

After obtaining initial guesses, the binned data are fitted to Lorentzians. Since the bin widths are chosen to be on the order of the expected FWHM, a time window corresponding to 20 bins around the expected signal time is used in the fit. The results on the binned data are used to inform a second fit on the unbinned, filtered data. The results of which are used to test consistency with a domain wall signal. The fit provides an estimation of the amplitudes, durations, and timings of the individual signals with their uncertainties.

The fit fails if the amplitude or duration is smaller than their respective uncertainty, because it would be unphysical for these quantities to be zero. Likewise, the fit fails if it does not converge to a solution. An amplitude of zero with an uncertainty equal to the standard deviation over the data segment is assigned to a failed fit. Note that no timing information can be obtained if the fit fails. However, an amplitude of zero still yields useful information, because this can occur if the wall's velocity is orthogonal to the sensitive axis of a sensor. The different steps in the fit procedure are shown in Fig. 4 for a simulated signal. Additionally, one could consider a goodness-of-fit statistic, such as the χ^2, to determine if a fit fails. However, these statistics are sensitive to deviations from a Lorentzian shape. Since the specific line-shape is not of interest, these statistics are not used.

2.3.2 Fit to the domain-wall crossing model

After fitting the individual signals, the information extracted (timing, amplitude, and duration) from each sensor is checked for consistency with a planar domain wall traversing the Earth. The magnitude and velocity of a wall crossing will determine the amplitude and timing of the observed signals across the GNOME sensors. The amplitudes of the signals detected by the individual sensors depend on the nominal magnitude m as well as the relative direction $\hat{\boldsymbol{v}}$ of the wall crossing compared to the sensitive axes of the detectors $\hat{\boldsymbol{d}}_i$. Similarly, the timing of the signal in the individual magnetometers is determined by the domain-wall's velocity and the location of the detectors.

The measured amplitudes $\{s_i\}$ from the GNOME sensors yields information about the magnitude of a wall event. The nominal amplitude m is suppressed by the factor κ_i as expressed in Eq. (5). That is, for $\boldsymbol{m} \equiv m\hat{\boldsymbol{v}}$, the observed signal in a single sensor is $s_i = \kappa_i m = \hat{\boldsymbol{d}}_i \cdot \boldsymbol{m}$. For all of the sensors, the measured

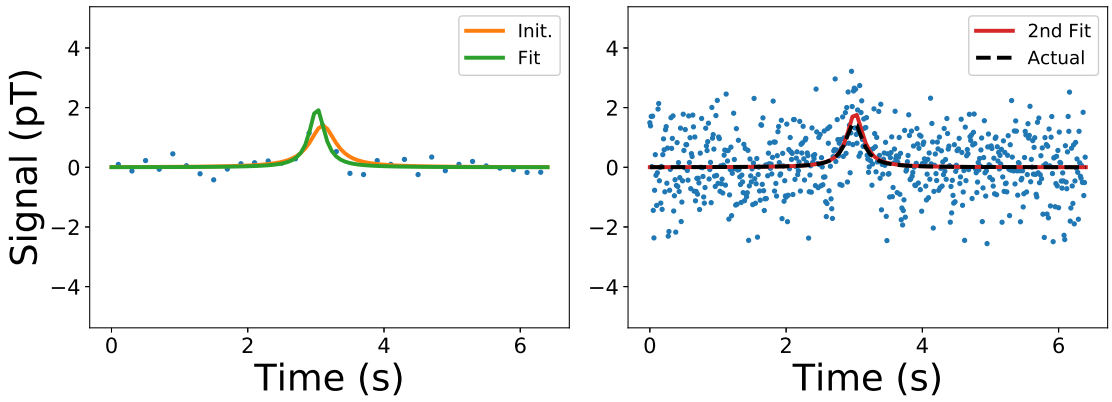

Figure 4: Fitting simulated data in three steps: (left, orange) initial guess, (left, green) fitting to binned data, then (right, orange) fitting to unbinned data.

amplitude can be written in matrix form,

$$D\boldsymbol{m} = \boldsymbol{s} \quad \text{for } D \equiv \begin{bmatrix} \hat{\boldsymbol{d}}_1^T \\ \hat{\boldsymbol{d}}_2^T \\ \vdots \\ \hat{\boldsymbol{d}}_n^T \end{bmatrix}, \; \boldsymbol{s} \equiv \begin{bmatrix} s_1 \\ s_2 \\ \vdots \\ s_n \end{bmatrix} . \tag{10}$$

The covariance matrix for the signal vector $\boldsymbol{s}$ are denoted with Σ_s. This matrix describes the uncertainty in the signal amplitude from fitting the individual signals to Lorentzians. The residual is defined by $\boldsymbol{r} = D\boldsymbol{m} - \boldsymbol{s}$. The vector $\boldsymbol{m}$ is determined by minimizing the χ^2 given by

$$\chi^2_{\text{fit0}} = \boldsymbol{r}^T \Sigma_s^{-1} \boldsymbol{r} . \tag{11}$$

Equation (11) is solved by

$$\boldsymbol{m} = \Sigma_m D^T \Sigma_s^{-1} \boldsymbol{s} \quad \text{for} \quad \Sigma_m = (D^T \Sigma_s^{-1} D)^{-1} . \tag{12}$$

The corresponding magnitude of the domain wall is then

$$\|\boldsymbol{m}\| \pm \frac{1}{\|\boldsymbol{m}\|} \sqrt{\boldsymbol{m}^T \Sigma_m \boldsymbol{m}} . \tag{13}$$

Timing data can be used to determine the velocity of the wall. However, in order to determine timing, a signal must be found; so signals with negligible amplitude do not contribute timing information. The timing must also be taken relative to some sensor. Thus, to guarantee that an array of (perfect) detectors finds a signal, the array must consist of at least six detectors in different locations with different orientation (such that no more than two vectors are coplanar for both the relative location and the sensitive axes): up to two sensors could be insensitive to some direction, one sensor is used as a reference point, and at least three other sensors with wall timing data are needed.

The time difference between the transient signals observed in two magnetometers is given in Eq. (4). Consider a set of n' relative times $\{\Delta t_i\}$ and positions $\{\boldsymbol{\Delta x_i}\}$. One then obtains an equation analogous to Eq. (10):

$$X \left(\frac{\boldsymbol{v}}{\|\boldsymbol{v}\|^2} \right) = \boldsymbol{t} \quad \text{for } X \equiv \begin{bmatrix} \boldsymbol{\Delta x}_1^T \\ \boldsymbol{\Delta x}_2^T \\ \vdots \\ \boldsymbol{\Delta x}_{n'}^T \end{bmatrix}, \; \boldsymbol{t} \equiv \begin{bmatrix} \Delta t_1 \\ \Delta t_2 \\ \vdots \\ \Delta t_{n'} \end{bmatrix} . \tag{14}$$

This system can be solved for $\frac{\boldsymbol{v}}{\|\boldsymbol{v}\|^2}$ in the same manner as described in Eq. (10). The resulting vector, $\frac{\boldsymbol{v}}{\|\boldsymbol{v}\|^2}$, is in the direction of the wall's velocity, but with norm given by the inverse speed.

Solving the linear equation for $\frac{\boldsymbol{v}}{\|\boldsymbol{v}\|^2}$, one obtains:

$$\frac{\boldsymbol{v}}{\|\boldsymbol{v}\|^2} = \Sigma_{1/v} X^T \Sigma_t^{-1} \boldsymbol{t} \quad \text{for} \quad \Sigma_{1/v} = (X^T \Sigma_t^{-1} X)^{-1} \ , \tag{15}$$

where Σ_t is the covariance matrix for the relative timing data. These uncertainties are extracted after fitting the individual signals to Lorentzians. Observe that there is correlation in the relative times because they all use the same reference time. Thus, Σ_t has nonzero off-diagonal terms. The speed of the wall and its uncertainty are then

$$v = \|\boldsymbol{v}\| \pm \|\boldsymbol{v}\|^2 \sqrt{\hat{\boldsymbol{v}}^T \Sigma_{1/v} \hat{\boldsymbol{v}}} \ . \tag{16}$$

One can calculate χ^2_{fit1} analogously to Eq. (11) as,

$$\chi^2_{\text{fit1}} = \boldsymbol{r_t}^T \Sigma_t^{-1} \boldsymbol{r_t} \ , \tag{17}$$

with the residuals $r_t = X \left(\frac{\boldsymbol{v}}{\|\boldsymbol{v}\|^2} \right) - \boldsymbol{t}$.

The two systems of equations described in this section can be simultaneously solved by combining them with a direct sum. That is, the magnitude and velocity calculations are combined as

$$(D \oplus X) \left(\boldsymbol{m} \oplus \frac{\boldsymbol{v}}{\|\boldsymbol{v}\|^2} \right) = (\boldsymbol{s} \oplus \boldsymbol{t}) \ . \tag{18}$$

The direct sum allows one to include correlated errors between amplitude and timing and determine the correlation between the magnitude and velocity vectors. When finding the vector $\boldsymbol{m} \oplus \frac{\boldsymbol{v}}{\|\boldsymbol{v}\|^2}$ that minimizes the χ^2, a combined covariance matrix Σ_{st} — similar to $\Sigma_s \oplus \Sigma_t$, but with correlations between $\boldsymbol{s}$ and $\boldsymbol{t}$ — is considered. The matrix Σ_{st} also includes correlations between the magnitude and timing for each signal. Solving this system yields a single, combined χ^2 parameter,

$$\chi^2_{\text{fit}} = \boldsymbol{r}_{st}^T \Sigma_{st}^{-1} \boldsymbol{r}_{st} \ , \tag{19}$$

for the residual $\boldsymbol{r}_{st} = (D \oplus X) \left(\boldsymbol{m} \oplus \frac{\boldsymbol{v}}{\|\boldsymbol{v}\|^2} \right) - (\boldsymbol{s} \oplus \boldsymbol{t})$, as well as two vectors for the magnitude $\boldsymbol{m}$ and velocity $\boldsymbol{v}$ calculation. The χ^2_{fit} is expected to follow the underlying χ^2 distribution. Therefore, the p-value is defined as the probability of obtaining a χ^2_{fit} value equal or larger than the one found. Larger p-values indicate a better agreement with the model. One demands that the p-value corresponding to χ^2_{fit} be above some threshold for a potential event to be considered consistent with a domain-wall crossing. The specific value of the threshold is defined in Sec. 3.

Earth-based sensors are only stationary in the accelerated (rotating) reference frame. For Earth's radius ($\approx 6.371 \times 10^6$ m), rotation period (1 day), and a domain-wall velocity of $v \approx 3 \times 10^5$ m/s, according to numerical calculations, the effects of the Earth's rotation on the timing between two sensors would be $\Delta t \lesssim 33$ ms, while the Earth's rotation will modulate a signal of amplitude m by $\frac{\Delta m}{m} \lesssim 0.003$. Though rotation may have little effect on the magnitude results, it may have a measurable effect on the timing, because the GNOME magnetometer bandwidths can resolve this time difference.

Up to first-order corrections to the velocity, the timing for each sensor is given by $\boldsymbol{\Delta x_i} \cdot \frac{\boldsymbol{v}-\boldsymbol{\delta v}}{\|\boldsymbol{v}-\boldsymbol{\delta v}\|^2} = \Delta t_i$ for tangential velocity in the direction of the wall $\boldsymbol{\delta v}$. This equation is no longer linear with respect to $\boldsymbol{v}$ (or something proportional to this). Thus correcting for the rotating Earth demands solving a non-linear problem. The first-order correction reduces the relative time error to $\Delta t \lesssim 0.05$ ms; well below the bandwidth of the GNOME magnetometers. In practice, a first approximation is made by solving the linear problem assuming that the Earth is stationary and using that solution as an input to the non-linear problem. Standard propagation of errors is used to determine the final statistics.

2.3.3 Directional consistency

The directions of $\boldsymbol{m}$ and $\frac{\boldsymbol{v}}{\|\boldsymbol{v}\|^2}$ can be compared by considering the angle between the two vectors (see Fig. 11). One would expect these two vectors to be in the same direction if the signals are consistent with a domain

wall. The angle is determined by first defining the orientation of a plane spanned by the two vectors. The angle between the vectors is then defined with respect to the orientation of the plane. The angle must be given with respect to an oriented plane because comparing the absolute angle between two vectors would cause indeterminant statistics; i.e., when the vectors are in nearly the same direction, a small perturbation in one of the vectors would cause a negligible perturbation in the angle, up to first order. A full derivation of the angle is given in App. A. For a real event, the angle between the vectors should be zero. One can obtain a χ^2 statistic from the ratio between the measured angle and its uncertainty.

The covariance matrix can be constructed using the uncertainties on $\boldsymbol{m}$ and $\frac{\boldsymbol{v}}{\|\boldsymbol{v}\|^2}$ given in the previous section. The uncertainties in the angle follows from propagation of errors (see App. A). The agreement in the direction of $\boldsymbol{m}$ and $\frac{\boldsymbol{v}}{\|\boldsymbol{v}\|^2}$ can be quantified with

$$\chi^2_{\rm dir} = (\Delta\theta)^2/\sigma^2_{\Delta\theta} \ , \tag{20}$$

which has two degrees of freedom, where $\Delta\theta$ is the angle between the two vectors and $\sigma_{\Delta\theta}$ is the uncertainty in the angle defined in Eq. (29).

2.3.4 Duration consistency

The duration of the signal in each sensor is expected to be the same and equal to the domain-wall crossing duration τ. Thus, one would want to compare the measured duration τ_i as measured by some sensor to τ. However, since the exact duration is not known, one must consider instead the $\bar{\tau}$ that minimizes

$$\chi^2_{\rm dur} = \sum_{i=1}^{n'} \frac{(\tau_i - \bar{\tau})^2}{\sigma^2_{\tau_i}} \ , \tag{21}$$

where σ_{τ_i} is the uncertainty in τ_i, and the n' signal duration measurements are assumed to have uncorrelated errors. The $\chi^2_{\rm dur}$ is minimized for the weighted mean,

$$\bar{\tau} = \frac{\sum_{i=1}^{n'} \tau_i/\sigma^2_{\tau_i}}{\sum_{j=1}^{n'} 1/\sigma^2_{\tau_j}} \ . \tag{22}$$

For n' duration measurements, agreement between the durations is characterized by $\chi^2_{\rm dur}$ with $(n'-1)$ degrees of freedom.

The effects of filtering may modify the observed signal width. Though this would not be a significant concern for signals that are filtered in the same way, different filters may change the signal width differently. For example, some sensors may have notch filters at 50 Hz while others have notch filters at 60 Hz to remove noise from the electrical grid. However, the differences due to different filter choice are assumed to be negligible for this analysis.

2.3.5 Combining the consistency checks

In order to verify that the consistency checks can characterize the agreement between the data and the model, a large number of simulated signals were analyzed. The statistics of the χ^2 values corresponding to each consistency check are obtained and then compared to the expected χ^2 distributions. Since the χ^2 values agree with the expected distribution, a p-value can be assigned to the result of each consistency check. The three p-values are combined as a product to define the acceptance threshold.

For each sensor, the simulated sample consisted of a wall event from a random direction and Gaussian noise based on the Gaussian noise background described in Table 1. Other parameters (signal width, amplitude, and speed) are set to be constant. For simplicity, the filters are not applied, and the uncertainty in the signal is given directly by the chosen Gaussian noise. Signals are fitted to Lorentzian curves, and this information is tested for consistency with an expected signal.

The distributions of statistics are given in Fig. 5. These are in rough agreement with the expected χ^2 distributions. For all cases, there are some instances in which the χ^2 value is very large. This may be due to fitting to a peak in the noise. Imperfect fits are likely the cause of the small deviation from the expected χ^2

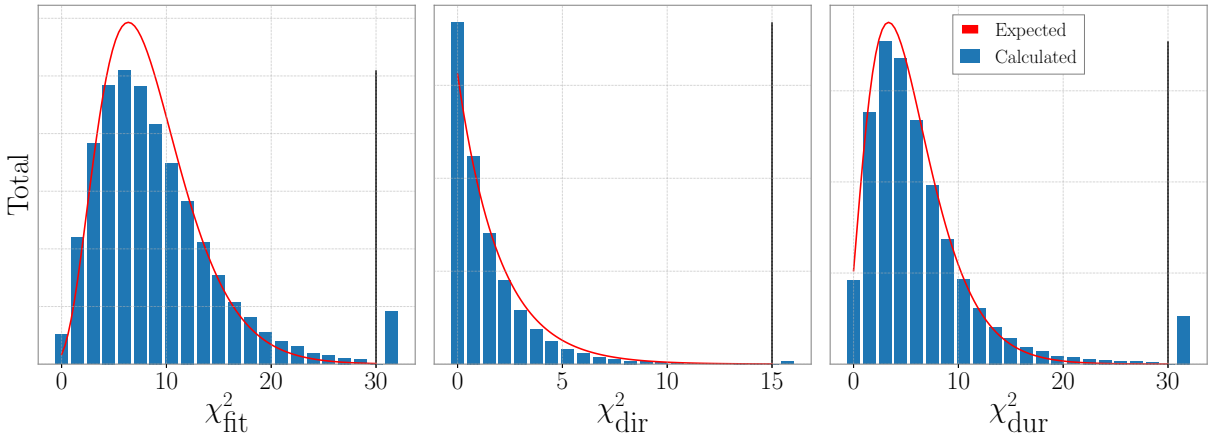

Figure 5: Distribution of statistics from the consistency checks: histograms of (left) χ^2_{fit} distribution from obtaining velocity and magnitude vectors, (middle) χ^2_{dir} distribution from comparing the directions of the magnitude and velocity vectors, and (right) χ^2_{dur} distribution from comparing measured widths. In all plots, the entry right of the black vertical line represents the total number of entries right of that line, and the expected distribution is in red.

distributions. Regardless, the rough agreement suggests that the χ^2 from the consistency check adequately describes the agreement between the data and the model. Thus, these statistical measurements can be used to accept or reject potential wall events.

The p-value (i.e., the probability of obtaining a χ^2 value greater than what was measured) is used to quantify the agreement to the domain-wall model. The p-value is the probability that the deviation from the model (in this case, a domain-wall event) can be explained by the uncertainty in the measurement. Thus, a small p-value means that the potential event is significantly inconsistent with a domain wall. The output of each consistency check presented previously is combined using the product $p_{\text{prod}} \equiv p_{\text{fit}} \times p_{\text{dir}} \times p_{\text{dur}}$, corresponding to the χ^2 from Eqs. (19), (20), and (21), respectively. Then the agreement of a candidate event to a domain-wall crossing is quantified by one parameter, p_{prod}. Using the product of the p-values is largely arbitrary. One can argue that the product of p-values is a reasonable choice, since this would be roughly the probability of passing all consistency checks, ignoring correlation. In any case, the relevant parameters in choosing a cut-off are the false positive and false negative rates (described in Sec. 3), so any underlying meaning of the cut-off parameter is not relevant. In addition to the cut-off, if there are not enough data to perform all consistency checks, then the potential event is rejected.

2.4 Network sensitivity

In order to define the detection capabilities of GNOME, a notion of sensitivity must be established. Defining the matrix D and magnitude vector $\boldsymbol{m}$ as in Eq. (10), one can define a function $\mathcal{A}$ that takes the signal-to-noise ratio from each sensor $\Sigma^{-1/2}D\boldsymbol{m}$ and returns a collective signal-to-noise ratio[2].

The output of this function is compared to some threshold α for finding a wall event. For example, if $\mathcal{A}(\Sigma^{-1/2}D\boldsymbol{m}) \geq \alpha$ for the event, then a signal is found, otherwise it is missed. Thus, the exact definition of $\mathcal{A}$ is based on the analysis method. For the analysis described here, one finds signals by searching for instances in which the weighted mean of multiple measurements exceeds some signal-to-noise threshold. Using the weights from Eq. (6) and the uncertainty from Eq. (7), one finds $\mathcal{A}(\Sigma^{-1/2}D\boldsymbol{m}) = \|\Sigma^{-1/2}D\boldsymbol{m}\|$, i.e., $\mathcal{A}$ is simply the Euclidean norm.

The sensitivity of the system can be defined as the minimum signal needed to guarantee that the signal-to-noise is at least one. The sensitivity in the direction $\hat{\boldsymbol{m}}$ is obtained by solving $\mathcal{A}(\Sigma^{-1/2}D\beta\hat{\boldsymbol{m}}) = 1$ for

[2] $\Sigma^{-1/2}$ is well-defined because Σ is always positive definite. For uncorrelated uncertainties, $\Sigma^{-1/2} = \text{diag}\left\{\frac{1}{\sigma_i}\right\}$.

β:

$$\beta(\hat{\boldsymbol{m}}) \equiv \frac{1}{\mathcal{A}(\Sigma^{-1/2} D\hat{\boldsymbol{m}})} \ , \tag{23}$$

since $\mathcal{A}$ is absolutely scalable — i.e., $\mathcal{A}(\beta\hat{\boldsymbol{m}}) = |\beta|\mathcal{A}(\hat{\boldsymbol{m}})$. Thus, if $\beta(\hat{\boldsymbol{m}})$ is large, then a large magnitude is needed to induce a measurable signal in the direction $\hat{\boldsymbol{m}}$. An example of the network sensitivity is plotted in Fig. 6 in geocentric coordinates. The configuration of the sensors is described in Table 1. A clear pattern can be observed where the network is more sensitive to certain directions. An ideal configuration would show an homogeneous sensitivity in all directions.

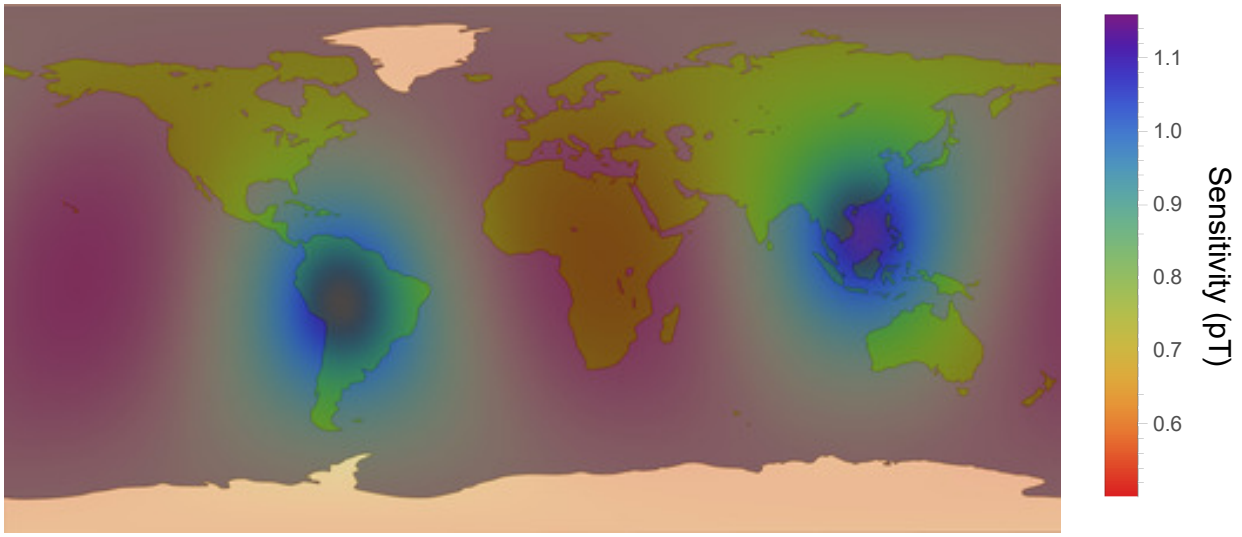

Figure 6: Directional sensitivity of the network according to the configuration used to generate simulated data (see Table 1). The color overlayed on the map of the Earth is $\beta(\hat{\boldsymbol{m}})$ from Eq. (23), where the position on the map corresponds to the first contact point of a domain wall on the Earth's surface.

To reduce $\beta(\hat{\boldsymbol{m}})$ to a single number, one could assume a distribution of signals based on some model (e.g., the SHM) and take the weighted average of the sensitivity over the signal distribution. Alternatively, one could achieve a sensitivity bound by considering the worst-case scenario in which β is maximized. When $\mathcal{A}$ is the vector norm, this amounts to solving the eigenvalues of $\Sigma^{-1/2}D$. Denote $\lambda_{\rm min}$ as the smallest eigenvalue and $\hat{\boldsymbol{x}}_{\rm min}$ as the corresponding eigenvector. Then the sensitivity in the worst direction is $1/\lambda_{\rm min}$ for the worst direction $\hat{\boldsymbol{x}}_{\rm min}$. Note that the optimal orientation for an additional sensor would be $\hat{\boldsymbol{x}}_{\rm min}$ in any location.

In addition to the sensitivity of the network, the resolution for relative time measurements can be improved by spreading out the location of the sensors. Assuming that the clocks are stable over the measurement time, increasing the delay of the event observations by increasing the distance between the sensors will proportionally improve the timing resolution. For example, a fast domain wall may not have a measurable delay unless the sensors are sufficiently separated to resolve the small difference in timing. Improving the timing resolution may lead to a better calculation of the velocity and improvements in the consistency checks, but it would not lead to detecting any additional events.

3 Testing analysis methods

The algorithm presented depends on two thresholds to identify domain-wall events: the signal-to-noise ratio thresholds and the product of p-values from the consistency check. The study of the false negatives and false positives rates allows one to determine the thresholds needed to achieve a specific confidence level of detection. The rate of false negatives defines how reliable the algorithm is in identifying events. Meanwhile, the rate of false positives defines the probability of identifying a feature arising in the noise as a real domain-wall event. In this section, simulated data are used to determine appropriate thresholds based on the rate of false positives and false negatives.

3.1 False negatives analysis

The false negatives rate describes the analysis procedure's ability to identify real signals. In order to quantify this, simulated data with inserted signals are analyzed. False negative rates are calculated for both the search algorithm and the consistency check.

The search algorithm is particularly sensitive to events that reproduce the expected pattern and flags them if they feature a significant signal-to-noise ratio. Due to the binning procedure, the apparent amplitude of the event depends on its duration given by Eq. (3). An example showing the detection probability is given in Fig. 7. In this figure, 3.6×10^4 domain walls are simulated with different amplitudes and durations. For each simulated sample, a domain wall was insert with a random direction and constant speed. The search algorithm is performed with a threshold of 5σ. This shows that the detection probability is close to 90 % for signals with a magnitude above the threshold. The red and blue lines show the detection limits considering the attenuation given by Eq. (3). Note that the search algorithm identifies the inserted domain-wall event but possibly also other peaks in the noise. Therefore, the consistency check to the domain-wall crossing model is required to remove the additional events.

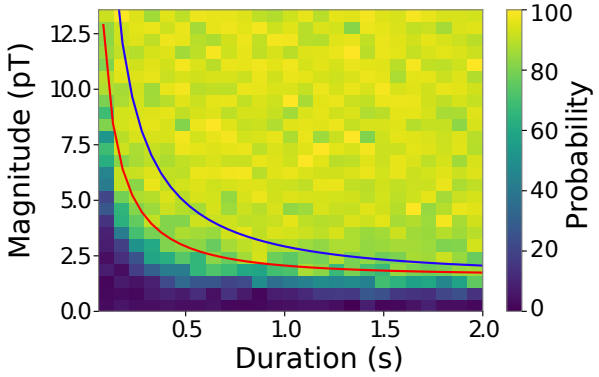

Figure 7: Probability of finding an inserted domain-wall event in simulated data depending on the magnitude and the duration of the wall. Table 1 describes the characteristics of the simulated network. The lines indicate the bounds on the event magnitude required to find a signal with 5σ signal-to-noise ratio.

After the events are flagged, they are scrutinized for consistency with the domain-wall crossing model. As reported in Sec. 2.3, the agreement of an event with a domain-wall crossing can be quantified by the product of p-values, i.e., an event is inconsistent with a domain wall if the product is less than some threshold. When a high p-value is required, the agreement to the model is more stringent. Even though this increases the confidence of correctly identifying a real signal, it also increases the probabilities of missing a real signal. On other hand, allowing lower p-values produces fewer rejections; lowering the false negative rate but increasing the chances of misidentifying a false event. The probability of detecting a given real signal is described in Fig. 8. The domain-walls are generated with fixed magnitude, duration, and speed, while the incoming direction is randomized. Table 1 describes the network characteristics. The time when the events are inserted is given as initial guess to the consistency check algorithm. Figure 8 is generated with 10^5 simulated samples. One can see how the probability of detection changes with the p-value requirement. The rate of false negatives decreases exponentially as the p-value decreases. As an example, the false negative rate is 4 % for a p-value product of 10^{-5}. Meaning that 96 % of real events would be detected.

3.2 False positive analysis

Considering only noise in the data, there is some probability that random spikes mimic a domain-wall crossing. This will limit the discovery capabilities of the network. Taking the convention from particle physics, a domain wall found should have a 5σ significance to be accepted — i.e., 1 in 1.7 million chance of a false positive over the course of the measurement.

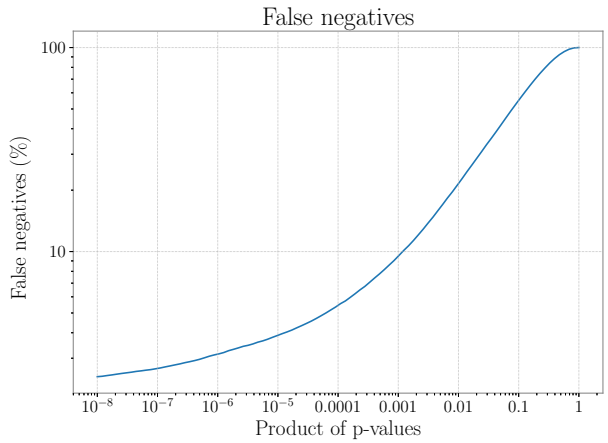

Figure 8: The percentage of rejected simulated events as a function of the product of p-values.

The rate of false positives is quantified for the noise characteristics shown in Table 1. Gaussian noise was generated for each sensor. The simulated data were analyzed for domain-wall crossings using both the search algorithm and the consistency check. Since no signals were injected into the simulated noise, all potential wall-crossing events must be false positives.

The rate of false positives is expected to follow Poissonian statistics. Namely, the probability that one finds n_f false positives over an interval of duration t, where the rate of false positives, r, is given by

$$P(n_f; rt) = e^{-rt} \frac{(rt)^{n_f}}{n_f!} \ .$$

For an interval $T_{\rm samp}$ of data, if n_f false positives are found, the upper-bound on the rate $r_0 \geq r$ at a confidence level C is given by solving

$$C = \int_0^{r_0 T_{\rm samp}} P(n_f; x) dx \ .$$

The probability of finding a false positive over the course of a t-long run is then

$$P_{\rm FP} \leq 1 - e^{-r_0 t} \ . \tag{24}$$

The rate of false positives was calculated using 10^4 days of simulated noise data at 512 Hz and binning at 1 s. The signal-to-noise thresholds change the number of potential events flagged by the search algorithm. The consistency check can reject these events either because the p-value product was too low or because there were not enough data to evaluate all the p-values. In particular, if there is not enough timing data to calculate the wall's velocity, the event is rejected. This can occur when fewer than four magnetometers feature a peak that is prominent enough to measure its timing. If the velocity estimated from the timing data can be calculated, all consistency checks can be performed. The rate of false-positive data that pass the consistency check for different thresholds is summarized in Fig. 9. One observes that about 99.8 % of the events are rejected simply because there is not enough data for the consistency check. Using a 5σ signal-to-noise threshold yields no potential events. This puts a limit of 0.08 events per year. For one month of data, there would be up to a 0.7 % chance of finding a false positive under this threshold (for any p-value product threshold).

However, if one wants to demand the standard 5σ significance on the false positive event rate (at 90 % confidence) using simulated signals, one would need to simulate over 4 million times as much data as one wants to measure and choose thresholds such that no events are found. This is computationally impractical. Instead, bounds on the rate as a function of the thresholds can be extrapolated from a more modest sample size. Holding the p-value threshold constant, one finds the rate to scale exponentially with the signal-to-noise

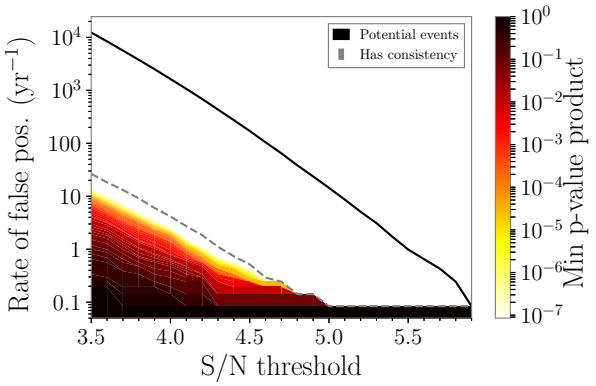

Figure 9: Upper bounds on false positive rate (90 % confidence) for different thresholds. The data consist of 10^4 days of simulated Gaussian noise from nine sensors based on expected noise. The thresholds include the signal-to-noise ratio needed for the search algorithm (x-axis) and the product of p-values from the consistency check (color gradient).

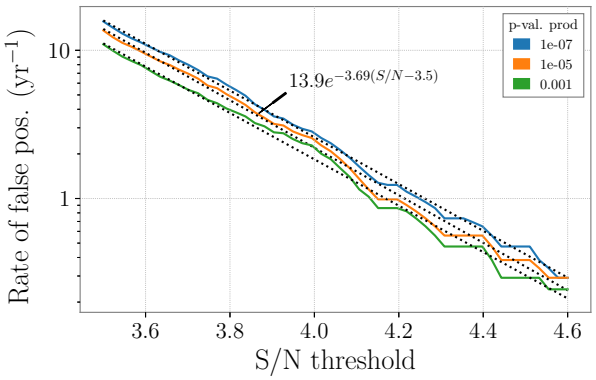

Figure 10: The rate of false positives as a function of the signal-to-noise threshold used to find potential wall events and keeping the threshold used to verify events constant.

threshold (Fig. 10). Extrapolating the rate of false positives for the threshold $p_{\text{prod}} > 10^{-5}$, one would need to demand a signal-to-noise threshold of at least 7.5 to achieve a 5σ significance in detection.

If no events are found above this threshold, the detection limit would be defined by the strongest event found. If the strongest event is found at, say, 4.5σ, no detection can be claimed, because such a signal may be due to random noise. However, one can be sure that no event stronger than 4.5σ occurred during the course of the measurement. Therefore, this can be taken as a new bound for the sensitivity of the network. Based on the sensitivity $\beta \sim \sigma$ from Eq. (23), no domain-wall event would have been detected with magnitude strictly greater than 4.5β, averaged over all directions, over the duration of the measurement. This improves on the initial sensitivity limit of 7.5β set by the 5σ significance condition.

4 Conclusions

In this paper, an analysis method for finding and verifying domain-wall signals in GNOME is presented in detail. Candidate signals are identified by first time-shifting the data to align the signals in different sensors according to an incoming event velocity. Then the data from different GNOME sensors are combined using a weighted mean. Combining the data is dependent on the velocity of the event, so a range of possible velocities is scanned.

The potential signals are scrutinized for consistency with a domain-wall crossing. The signals in each sensor are measured to obtain their amplitude, timing, and duration. The timing and amplitude information is used to obtain the most likely magnitude, speed, and direction of the candidate domain wall, as well as statistics for how well the signals agree with the most likely domain-wall characteristics. The fit performed to the wall crossing model provides two directions corresponding to the velocity and magnitude of the domain-wall event. These are expected to agree (up to a sign); so the statistical agreement between these directions provides an additional consistency check. Additionally, testing for agreement between the widths provides a third consistency check.

The analysis algorithm demands various thresholds for determining if features in the data were significant. For the finding algorithm, one considers the signal-to-noise ratio needed to find potential events. The chosen signal-to-noise threshold directly affects the sensitivity of the network when applying the analysis algorithm. For the consistency check, three different statistical measures are used to test agreement with a domain-wall crossing. A threshold was placed on the product of the three p-values.

The search algorithm and consistency check were tested using simulated data with Gaussian distributed noise. The simulated data inform appropriate thresholds to use for finding and verifying events. By demanding sufficiently stringent thresholds, the probability of identifying a noise feature as a real event can be made arbitrarily small. Likewise, the thresholds are chosen such that a real signal would not likely be rejected.

The methods used to calculate the false positive rate and false negative rate must be modified when applying to real data. The noise in real data may not have the same ideal distribution as used in the simulation. There are a few methods to generate realistic noise. For example, one could obtain a detailed characteristic of the noise, for example, the spectral density of the noise. These detailed characteristics would then be used to generate random noise. Alternatively, one could use data from the GNOME sensors. However, the data may contain signals, so measures are needed to ensure that the background does not contain any events. For example, one can sample the real data at random times for each sensor. Thus, a real event would not reproduce the expected pattern through network. Likewise, one could randomize the locations[3] of the sensors to effectively scramble any real signals when time-shifting the data.

Data from the GNOME magnetometers are now being analyzed using the methods described in this paper. The results of this analysis will be given in future publications.

Acknowledgements

We are sincerely grateful to Chris Pankow and Josh Smith for early contributions to the data analysis strategy and Andrei Derevianko, Ben Roberts, Conner Dailey, and Maxim Pospelov for valuable advice and insights. We are also thankful to all the members of the GNOME collaboration for useful discussions at many stages of development of the analysis procedure, especially H. Guo, T. W. Kornack, W. Li, M. Monroy, S. Nix, M. Padniuk, X. Peng, and D. Sheng.

This work was supported by the U.S. National Science Foundation under grants PHY-1707875 and PHY-1707803, the Swiss National Science Foundation under grant No. 200021 172686, and the European Research Council under the European Union's Horizon 2020 Research and Innovative Program under Grant agreement No. 695405.

References

[1] Paul Gorenstein and Wallace Tucker. Astronomical Signatures of Dark Matter. Advances in High Energy Physics, 2014:1–10, 2014.

[2] Jonathan L. Feng. Dark Matter Candidates from Particle Physics and Methods of Detection. Annual Review of Astronomy and Astrophysics, 48(1):495–545, 2010.

[3] Lars Bergström. Dark matter candidates. New Journal of Physics, 11, 2009.

[3]The orientation of the sensors could also be randomized. However, changing the relative orientation between the sensors would affect the sensitivity of the network.

[4] Gianfranco Bertone, Dan Hooper, and Joseph Silk. Particle dark matter: Evidence, candidates and constraints. Physics Reports, 405(5-6):279–390, 2005.

[5] Shigetaka Moriyama. Dark matter searches. AIP Conference Proceedings, 981:80–83, 2008.

[6] M. S. Safronova, D. Budker, D. Demille, Derek F.Jackson Kimball, A. Derevianko, and Charles W. Clark. Search for new physics with atoms and molecules. Reviews of Modern Physics, 90(2):25008, 2018.

[7] T Marrodan Undagoitia and L Rauch. Dark matter direct-detection experiments. ArXiv e-prints, 2015.

[8] Axel Lindner, Peter W. Graham, Steven K. Lamoreaux, Karl A. van Bibber, and Igor G. Irastorza. Experimental Searches for the Axion and Axion-Like Particles. Annual Review of Nuclear and Particle Science, 65(1):485–514, 2015.

[9] Y. V. Stadnik and V. V. Flambaum. Searching for dark matter and variation of fundamental constants with laser and maser interferometry. Physical Review Letters, 114(16):1–6, 2015.

[10] R. D. Peccei and Helen R. Quinn. CP conservation in the presence of pseudoparticles. Physical Review Letters, 38(25):1440–1443, 1977.

[11] Leanne D. Duffy and Karl Van Bibber. Axions as dark matter particles. New Journal of Physics, 11, 2009.

[12] A. Ringwald. Axions and Axion-Like Particles. ArXiv e-prints, 7 2014.

[13] P. Sikivie. Axions, domain walls, and the early universe. Physical Review Letters, 48(17):1156–1159, 1982.

[14] Masahiro Kawasaki, Ken'Ichi Saikawa, and Toyokazu Sekiguchi. Axion dark matter from topological defects. Physical Review D - Particles, Fields, Gravitation and Cosmology, 91(6):1–32, 2015.

[15] Sidney Coleman. Q-balls. Nuclear Physics B, 262(2):263–283, December 1985.

[16] Alexander Kusenko and Paul J. Steinhardt. Q -Ball Candidates for Self-Interacting Dark Matter. Physical Review Letters, 87(14), September 2001.

[17] D. F. Jackson Kimball, D. Budker, J. Eby, M. Pospelov, S. Pustelny, T. Scholtes, Y. V. Stadnik, A. Weis, and A. Wickenbrock. Searching for axion stars and Q -balls with a terrestrial magnetometer network. Physical Review D, 97(4):1–8, 2018.

[18] Abhishek Banerjee, Dmitry Budker, Joshua Eby, Hyungjin Kim, and Gilad Perez. Relaxion Stars and their detection via Atomic Physics. arXiv, February 2019.

[19] M. Pospelov, S. Pustelny, M. P. Ledbetter, D. F Jackson Kimball, W. Gawlik, and D. Budker. Detecting domain walls of axionlike models using terrestrial experiments. Physical Review Letters, 110(2):1–5, 2013.

[20] A. Friedland, H. Murayama, and M. Perelstein. Domain walls as dark energy. Phys. Rev. D, 67(4):043519, 2003.

[21] Katherine Freese, Mariangela Lisanti, and Christopher Savage. Colloquium: Annual modulation of dark matter. Reviews of Modern Physics, 85(4):1561–1581, 2013.

[22] Dmitry Budker and Michael Romalis. Optical magnetometry. Nature Physics, 3(4):227–234, 2007.

[23] S. Afach, D. Budker, G. DeCamp, V. Dumont, Z. D. Grujić, H. Guo, D. F. Jackson Kimball, T. W. Kornack, V. Lebedev, W. Li, H. Masia-Roig, S. Nix, M. Padniuk, C. A. Palm, C. Pankow, A. Penaflor, X. Peng, S. Pustelny, T. Scholtes, J. A. Smiga, J. E. Stalnaker, A. Weis, A. Wickenbrock, and D. Wurm. Characterization of the global network of optical magnetometers to search for exotic physics (GNOME). Physics of the Dark Universe, 22:162–180, 2018.

[24] Szymon Pustelny, Derek F Jackson Kimball, Chris Pankow, Micah P. Ledbetter, Przemyslaw Wlodarczyk, Piotr Wcislo, Maxim Pospelov, Joshua R. Smith, Jocelyn Read, Wojciech Gawlik, and Dmitry Budker. The Global Network of Optical Magnetometers for Exotic physics (GNOME): A novel scheme to search for physics beyond the Standard Model. Annalen der Physik, 525(8-9):659–670, 2013.

[25] D. F. Jackson Kimball, J. Dudley, Y. Li, S. Thulasi, S. Pustelny, D. Budker, and M. Zolotorev. Magnetic shielding and exotic spin-dependent interactions. Phys. Rev. D, 94(8):082005, 2016.

[26] M. Pospelov, J. Eby, Y. V. Stadnik, A. Wickenbrock, A. Weis, D. Budker, S. Pustelny, T. Scholtes, and D. F. Jackson Kimball. Searching for axion stars and Q -balls with a terrestrial magnetometer network . Physical Review D, 97(4):43002, 2018.

[27] B. M. Roberts, G. Blewitt, C. Dailey, and A. Derevianko. Search for transient ultralight dark matter signatures with networks of precision measurement devices using a Bayesian statistics method. Physical Review D, 97(8):83009, 2018.

A Statistical agreement between directions

In this study, the directions of the velocity and magnitude vectors must be in statistical agreement. Thus, an algorithm was designed to measure the angle between two vectors in an oriented plane. The propagation of errors is also calculated to determine if the angle between the vectors is negligible.

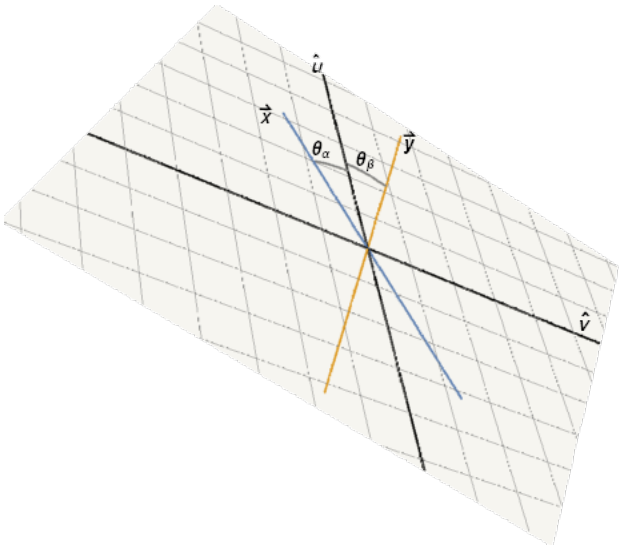

Figure 11: A visualization of how the directions of two vectors $\boldsymbol{x}$ and $\boldsymbol{y}$ are compared. The (oriented) angle $\Delta\theta = \theta_\alpha + \theta_\beta$ is measured in the plane spanned by the two vectors.

Consider the angle between some vectors $\boldsymbol{x}$ and $\boldsymbol{y}$. The first operation is to normalize the vectors $\boldsymbol{x} \mapsto \hat{\boldsymbol{x}} = \frac{\boldsymbol{x}}{\|\boldsymbol{x}\|}$ and $\boldsymbol{y} \mapsto \hat{\boldsymbol{y}} = \frac{\boldsymbol{y}}{\|\boldsymbol{y}\|}$. Next, an oriented plane containing $\boldsymbol{x}$ and $\boldsymbol{y}$ is defined so that the relative angle can be measured. Ideally, one of the axes defining the oriented plane would have a small angle with respect to $\boldsymbol{x}$ and $\boldsymbol{y}$. Labeling the axes of the plane $\hat{\boldsymbol{u}}$ and $\hat{\boldsymbol{v}}$, the angle of $\boldsymbol{x}$ and $\boldsymbol{y}$ relative to $\hat{\boldsymbol{u}}$ in the direction of $\hat{\boldsymbol{v}}$ will be measured. To define these axes, consider $\boldsymbol{w}_\pm = \hat{\boldsymbol{x}} \pm \hat{\boldsymbol{y}}$. Let $\hat{\boldsymbol{u}}$ be in the direction of the larger $\boldsymbol{w}_\pm$ and $\hat{\boldsymbol{v}}$ in the direction of the smaller. Then, the axes biject the angle between $\boldsymbol{x}$ and $\boldsymbol{y}$ with $\hat{\boldsymbol{v}}$ more perpendicular to $\boldsymbol{x}$ and $\boldsymbol{y}$.

The dot product with $\hat{\boldsymbol{v}}$ yields the sine of the desired angle. Define

$$\alpha = \sin\theta_\alpha \equiv \hat{\boldsymbol{x}} \cdot \hat{\boldsymbol{v}} \qquad \text{and} \qquad \beta = \mp \sin\theta_\beta \equiv \hat{\boldsymbol{y}} \cdot \hat{\boldsymbol{v}} \ . \tag{25}$$

Finally, the angle between the two vectors is given by

$$\Delta\theta = \arcsin\alpha \pm \arcsin\beta \ . \tag{26}$$

Propagation of errors is used to calculate the uncertainty in this angle. First, the Jacobian matrix for normalizing a vector $\boldsymbol{x}$ is

$$J^{\mathrm{n}}_{ij}(\boldsymbol{x}) = \frac{1}{\|\boldsymbol{x}\|^3}(\|\boldsymbol{x}\|^2\delta_{ij} - x_i x_j) \ . \tag{27}$$

The Jacobian matrix for the entire operation is then given by

$$J_{\Delta\theta} = \begin{bmatrix} \frac{1}{\sqrt{1-\alpha^2}} & \pm\frac{1}{\sqrt{1-\beta^2}} \end{bmatrix} \begin{bmatrix} \hat{\boldsymbol{v}}^T & 0 \\ 0 & \hat{\boldsymbol{v}}^T \end{bmatrix} \begin{bmatrix} J^{\mathrm{n}}(\boldsymbol{x}) & 0 \\ 0 & J^{\mathrm{n}}(\boldsymbol{y}) \end{bmatrix} \ . \tag{28}$$

With this, the statistics of the calculation can be determined. Given an initial covariance matrix Σ_{xy} for $\boldsymbol{x} \oplus \boldsymbol{y}$, the final variance is

$$\sigma^2_{\Delta\theta} = J_{\Delta\theta}\Sigma_{xy}J^T_{\Delta\theta} \ . \tag{29}$$

Agreement in the direction of $\boldsymbol{x}$ and $\boldsymbol{y}$ can be quantified with

$$\chi^2_{\mathrm{dir}} = (\Delta\theta)^2/\sigma^2_{\Delta\theta} \ , \tag{30}$$

which has two degrees of freedom.